© 2014. Published by The Company of Biologists Ltd | Journal of Cell Science (2014) 127, 3862–3876 doi:10.1242/jcs.155663

RESEARCH ARTICLE

Liprin-α1, ERC1 and LL5 define polarized and dynamic structures that are implicated in cell migration

Veronica Astro[1], Sara Chiaretti[1,*], Elisa Magistrati[1,*], Marc Fivaz[3] and Ivan de Curtis[1,2,‡]

ABSTRACT

Cell migration during development and metastatic invasion requires the coordination of actin and adhesion dynamics to promote protrusive activity at the front of the cell. The knowledge of the molecular mechanisms required to achieve such coordination is fragmentary. Here, we identify a new functional complex that drives cell motility. ERC1a (an isoform of ERC1) and the LL5 proteins LL5α and LL5β (encoded by *PHLDB1* and *PHLDB2*, respectively) are required, together with liprin-α1, for effective migration and tumor cell invasion, and do so by stabilizing the protrusive activity at the cell front. Depletion of either protein negatively affects invasion, migration on extracellular matrix, lamellipodial persistence and the internalization of active integrin β1 receptors needed for adhesion turnover at the front of the cell. Liprin-α1, ERC1a and LL5 also define new highly polarized and dynamic cytoplasmic structures uniquely localized near the protruding cell edge. Our results indicate that the functional complex and the associated structures described here represent an important mechanism to drive tumor cell migration.

KEY WORDS: Integrin, Invasion, Lamellipodia, Migration

INTRODUCTION

Cell migration is fundamental for development and tumor metastasis (Sahai, 2007; Vicente-Manzanares et al., 2009), and requires coordination of adhesion, cytoskeletal reorganization and membrane traffic (de Curtis and Meldolesi, 2012; Gauthier et al., 2012). An important question is how these processes are coordinated. Here, we investigated the mechanisms driving protrusion at the edge of cells migrating on or through extracellular matrix (ECM). We recently found that the adaptor protein liprin-α1 is required for efficient cell migration (Asperti et al., 2009). The liprin family includes four liprin-α and two liprin-β proteins that might form homo- and hetero-dimers, and might interact directly with several partners (de Curtis, 2011). The function of liprin-α proteins has been explored mainly in neurons, where they play a central role in regulating synaptic vesicle exocytosis (Stryker and Johnson, 2007).

Liprin-α1 is the most widely expressed member of the liprin-α proteins. Its polypeptide is highly expressed in human breast cancer and other types of human tumors (Rezaul et al., 2010; Astro et al., 2011). Moreover, liprin-α1 is needed for breast cancer cell motility and invasion *in vitro* (Astro et al., 2011), and is an important regulator of focal adhesion turnover and lamellipodial dynamics. To further dissect the role of liprin-α1 in cell motility, we have looked for relevant liprin-α1-interacting partners. Here, we have identified the adaptor proteins ERC1 (ELKS/Rab6-interacting/CAST family member 1) (Hida and Ohtsuka, 2010; Südhof, 2012) and LL5 (Paranavitane et al., 2003; Kishi et al., 2005) as important co-players, with liprin-α1, in the regulation of tumor cell migration and invasion. The ERC family (Nakata et al., 1999; Monier et al., 2002; Deguchi-Tawarada et al., 2004) includes ERC2, and two ERC1 isoforms, the brain-specific ERC1b and the widely expressed ERC1a (ELKSε) (Wang et al., 2002). In neurons, ERC proteins cooperate with liprin-α in the assembly of functional presynaptic sites (Dai et al., 2006). ERC1a interacts with LL5β (encoded by *PHLDB2*), a member of the LL5 family of adaptor proteins with a pleckstrin homology (PH) domain, which also includes LL5α (encoded by *PHLDB1*) and different splice variants. LL5β is part of a stable cortical platform at the periphery of the cell (Paranavitane et al., 2003; Lansbergen et al., 2006; Hotta et al., 2010; Takabayashi et al., 2010). Here, we found that ERC1a and LL5 proteins are needed, together with liprin-α1, to stabilize the edge of migrating cells and for the internalization of active integrins. Liprin-α1, ERC1a and LL5 colocalize near the protruding cell front, where they define new dynamic and highly polarized cytoplasmic structures that are specific to migrating cells. The PH domain of LL5 is required for the integrity of these assemblies and for efficient migration.

RESULTS

ERC1a and LL5 proteins are required for liprin-α1-mediated cell migration and invasion

Liprin-α1, ERC1a and LL5 proteins are co-expressed in invasive human breast cancer MDA-231 cells (Fig. 1A,B), and can be efficiently silenced with small interfering RNA (siRNA) (Fig. 1B,C; supplementary material Fig. S1A,B). In most experiments, we silenced both LL5α and LL5β to prevent compensatory effects. A complex between overexpressed liprin-α and ERC1, and endogenous ERC2–liprin-α complexes from synaptosomes have been identified (Ko et al., 2003). Recently a complex including liprin-α1, ERC and LL5 was identified at the cortex of non-motile HeLa cells (van der Vaart et al., 2013). Here, complexes containing co-transfected liprin-α1, ERC1a and LL5β were revealed (supplementary material Fig. S1C–E), suggesting that hetero-trimeric complexes might form in cells. However, we could not detect endogenous complexes. Given the dynamic nature of the compartment identified by these proteins, one possibility is that the interaction among the endogenous proteins undergoes a tight temporal regulation preventing the detectable accumulation of the complexes.

[1]Cell Adhesion Unit, San Raffaele Scientific Institute, 20132 Milano, Italy. [2]San Raffaele University, 20132 Milano, Italy. [3]Duke-NUS Graduate Medical School Singapore, 169857 Singapore.
*These authors contributed equally to this work

‡Author for correspondence (decurtis.ivan@hsr.it)

Received 24 April 2014; Accepted 6 June 2014

Journal of Cell Science

Journal of Cell Science (2014) 127, 3862–3876 doi:10.1242/jcs.155663

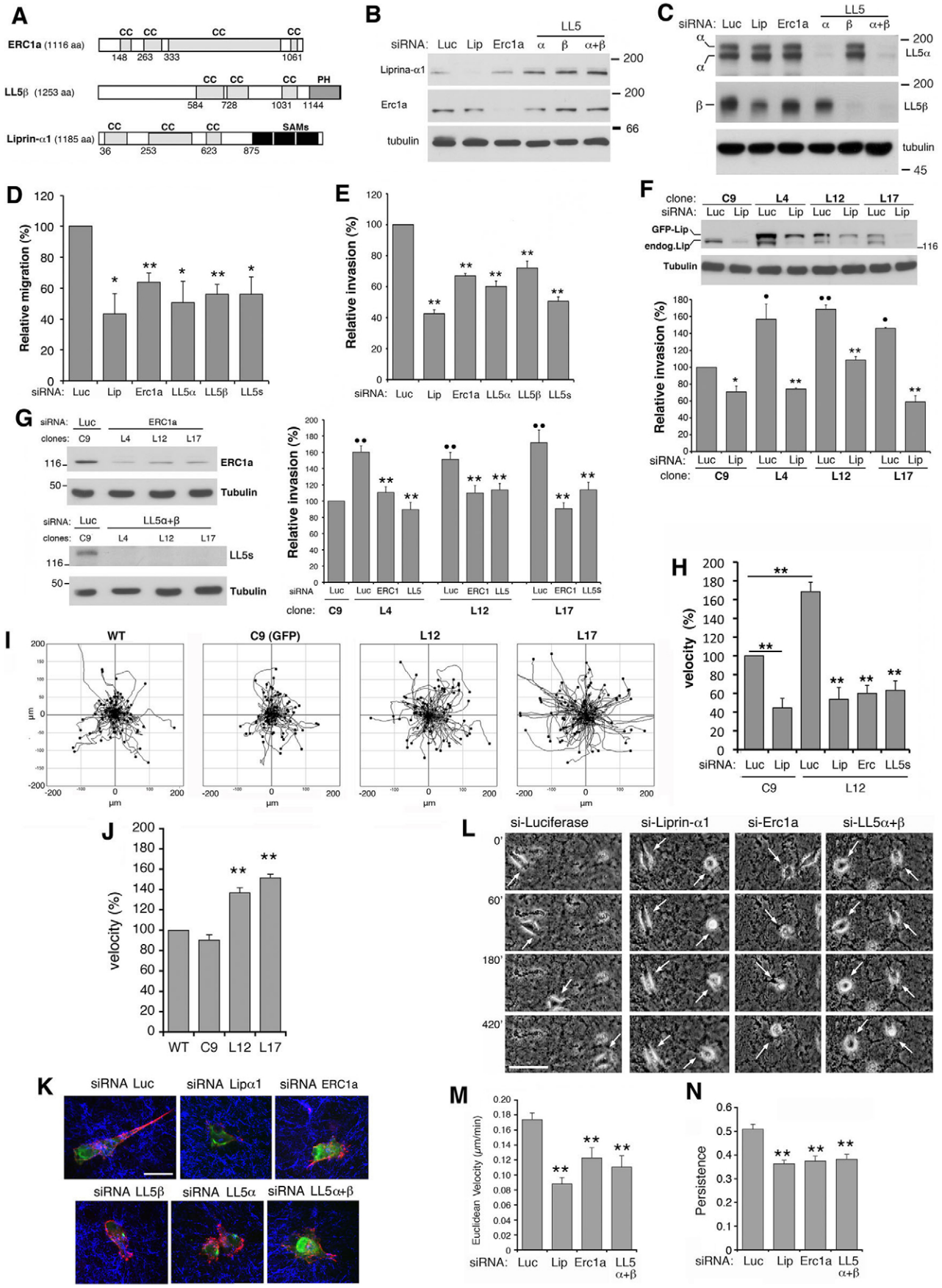

Fig. 1. See next page for legend.

Journal of Cell Science (2014) 127, 3862–3876 doi:10.1242/jcs.155663

Fig. 1. Liprin-α1, ERC1a and LL5 proteins are required for efficient invasion and migration through fibrillar matrices. (A) Human ERC1, LL5β and liprin-α1 proteins. CC, coiled coil; PH, pleckstrin homology; SAMs, sterile alpha motifs. (B,C) Blots for the endogenous proteins expressed in MDA-231 cells after transfection with control (Luc) or specific siRNAs. In C, two different antibodies specific for the indicated LL5 proteins (right) were used. (D,E) Effects of liprin-α1 (Lip), ERC1a or LL5 protein depletion (LL5s, both LL5α and LL5β) on haptotactic migration (D) and Matrigel invasion (E) by MDA-231 cells. Results are mean±s.e.m. normalized to control (n=4–6). (F) Top: immunoblotting for liprin-α1 in control C9 cells overexpressing GFP, and in three independent cell lines (L4, L12, L17) overexpressing GFP—liprin-α1. Cell lysates were from cells transiently transfected with the indicated siRNAs. Bottom: cell lines transfected with siRNAs were tested for invasion. Results are mean±s.e.m. (n=4–6). (G) Left: immunoblotting for ERC1a and LL5 in C9 cells and liprin-α1-overexpressing cells (L4, L12, L17) transfected with the indicated siRNAs. Right: control and liprin-α1-overexpressing cell lines transfected with indicated siRNAs were tested for invasion. Results are mean±s.e.m. (n=4–8 samples). *P<0.05, **P<0.005 compared with cells transfected with control siRNA; *P<0.05, **P<0.005 comparing liprin-overexpressing clones transfected with control siRNAs with C9 cells. (H) The increase in speed of migration on fibronectin of cells overexpressing liprin-α1 (L12) is prevented by silencing liprin-α1, ERC1 or LL5 proteins. Results are mean±s.e.m. normalized to control (n=37–53 cells). **P<0.005. (I) Plots with tracks of wild-type (WT), control (C9) and GFP–liprin-α1-expressing cells (clones L12, L17) migrating in fibroblast-derived matrices. Overexpression of liprin-α1 increases the speed of migration (J). Results are mean±s.e.m. normalized to control (n=72–87 cells); **P<0.005 compared with WT. (K) MDA-231 cells co-transfected with GFP and the indicated siRNAs were plated in fibroblast-derived matrices and fixed for immunofluorescence after 6 h. Scale bar: 20 μm. (L) MDA-231 cells transfected with siRNAs plated on fibroblast-derived matrices for 6 h were analyzed by time-lapse imaging. Arrows indicate the displacement of single cells with time. Scale bar: 100 μm. (M,N) Effects of the depletion of liprin-α1, ERC1a or LL5 proteins on the velocity and directionality of MDA-231 cells in 3D matrices. Results are means±s.e.m. (n=90–186 cells). **P<0.005.

As previously described for liprin-α1, depletion of ERC1a or LL5 inhibited MDA-231 cell spreading and migration on fibronectin (supplementary material Fig. S1F–H), as well as haptotactic migration and Matrigel invasion (Fig. 1D,E). The specificity of the effects of siRNAs was supported by reproducing similar effects on migration by a second set of siRNAs (supplementary material Fig. S1I). We isolated independent clones of MDA-231 cells overexpressing GFP–liprin-α1 (L4, L12 and L17 cell lines) or GFP (C9) (supplementary material Fig. S1K). These cells had viability and growth similar to control C9 cells (data not shown), but enhanced invasive abilities that were reversed by silencing endogenous and overexpressed protein (Fig. 1F). Liprin-α1-enhanced invasion was reduced by silencing ERC1a or LL5 (Fig. 1G). These data show a positive role of liprin-α1 in cell invasion and they imply that ERC1a and LL5 proteins have a role in liprin-α1-mediated motility. GFP–liprin-α1-expressing cells moved faster than control cells on two-dimensional (2D) fibronectin-coated substrates (supplementary material Fig. S1L,M). This effect was prevented by depletion of liprin-α1, ERC1a or LL5 (Fig. 1H, supplementary material Fig. S1N), indicating that these proteins are part of a functional network regulating migration.

We analyzed the effects of silencing either protein in a three-dimensional (3D) environment that more closely resembles the mesenchymal matrices met by invading cells *in vivo* (Cukierman et al., 2001). MDA-231 cells embedded in reconstituted ECMs had an elongated phenotype, with stretches of linear migration suggestive of movement along fibrillar structures (supplementary material Movie 1). Liprin-α1 overexpression enhanced the speed of migration in a 3D environment (Fig. 1I,J). Cells transfected with siRNAs against liprin-α1, ERC1a or LL5 were more rounded than control cells, with less pronounced leading processes and a defect in migration (Fig. 1K,L, supplementary material Movie 1). Although cells depleted of either protein could extend protrusions, these were unstable and the cells were impaired in their ability to move forward. Quantitative analysis confirmed their migration defect, with speed and directionality significantly affected after depletion of liprin-α1, ERC1a or LL5 (Fig. 1M,N).

Liprin-α1, ERC1a and LL5 proteins regulate lamellipodial dynamics

Silencing of ERC1a or LL5 proteins decreased the stability of lamellipodia (Fig. 2A), as previously observed after liprin-α1 silencing (Astro et al., 2011). Depletion of either protein induced the appearance of lamellipodia more frequently, but these lamellipodia were less persistent (Fig. 2B). The specificity of the effects of the different siRNAs was supported by reproducing similar decreases in the stability of lamellipodia with a second set of specific siRNAs (supplementary material Fig. S1J). In contrast, overexpression of liprin-α1 reduced the frequency and increased the stability of lamellipodia (Fig. 2C). These effects were also observed after the overexpression of ERC1a or LL5β (Fig. 2D). Interestingly, the potentiation of lamellipodial persistence by liprin-α1 overexpression was abolished not only by silencing liprin-α1 but also by silencing ERC1a or LL5 (Fig. 2C). Conversely, the instability of lamellipodia induced by silencing liprin-α1 was partially rescued by ERC1a overexpression (Fig. 2E).

Liprin-α1, ERC1a and LL5 colocalize at the front of migrating cells

Liprin-α1, ERC1a and LL5 proteins cooperate to regulate cell motility. Previous results have shown that these proteins colocalize in stable patches at the edge of nonmotile HeLa cells (Lansbergen et al., 2006; van der Vaart et al., 2013). Confocal analysis on migrating MDA-231 cells showed that endogenous ERC1a colocalized with liprin-α1 and LL5α near the edge of protrusions (Fig. 3A). ERC1a colocalized with LL5α and LL5β (Fig. 3B), and triple staining for ERC1a, liprin-α1 and LL5β confirmed their colocalization at clusters concentrated near lamellipodia in migrating cells (Fig. 3C). We next explored the dynamic localization of the transfected GFP-tagged proteins in cells migrating on fibronectin. As for the endogenous proteins, the overexpressed proteins were clearly concentrated near protruding lamellipodia (Fig. 3D). Time-lapse images showed a clear relationship between the presence of a protruding lamellipodium and the accumulation of the protein behind it (supplementary material Movie 2). Virtually all actively protruding lamellipodia analyzed (n=19–22 per construct) showed accumulation of liprin-α1, ERC1a or LL5 proteins.

The dynamic distribution in migrating cells indicates that the three proteins represent markers of highly dynamic functional cytoplasmic structures with a specific and polarized localization near the edge of active protrusions. Analysis of single lamellipodia showed that the concentration of ERC1a becomes evident soon after the protrusive activity starts, and that it is specifically localized behind the protruding lamellipodium. ERC1a-positive clusters disappear rapidly as the lamellipodium halts and starts to retract (Fig. 3E,F). Co-expressed mCherry- and

Journal of Cell Science (2014) 127, 3862–3876 doi:10.1242/jcs.155663

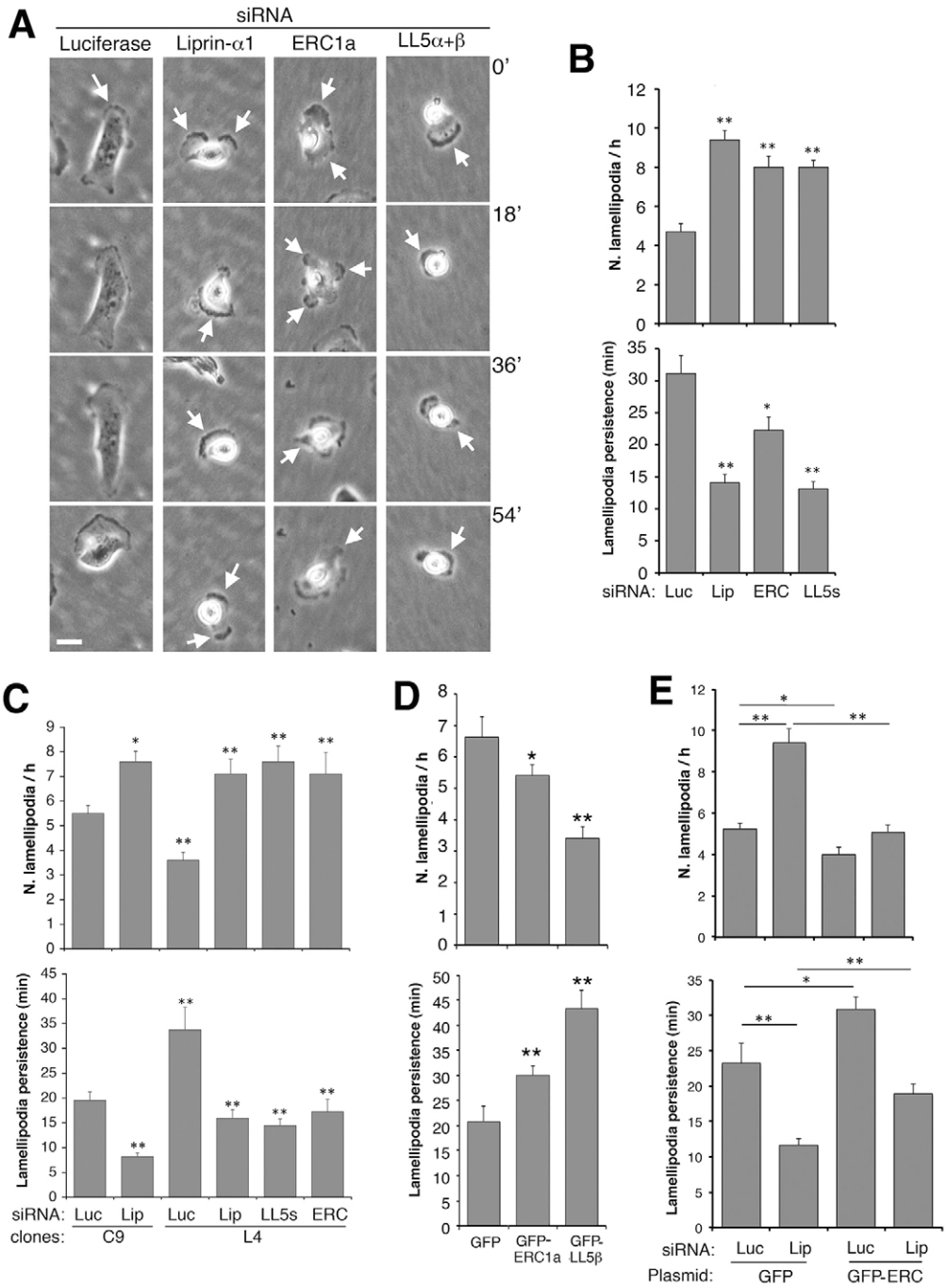

Fig. 2. Liprin-α1, ERC1a and LL5 proteins regulate the stability of lamellipodia. (A) Time lapse of MDA-231 cells on fibronectin. White arrows indicate the appearance of new protrusions in cells transfected with the indicated siRNAs. Scale bar: 10 μm. (B) Liprin-α1, ERC1a or LL5 silencing (Lip, liprin-α1; ERC, ERC1a; LL5s, both LL5α and LL5β) in cells migrating on fibronectin. Lamellipodial stability is reduced compared to transfection with control siRNA (Luc). Results are mean±s.e.m. (n=10 cells). (C) Cells overexpressing liprin-α1 (L4) produce less frequent and more stable lamellipodia compared to control (C9) cells. Effects of liprin-α1 overexpression are abolished by silencing liprin-α1, ERC1a or LL5 proteins. Results are mean±s.e.m. (n=10 cells). (D) Overexpression of ERC1a or LL5β decreases the frequency of lamellipodia formation and increases lamellipodial persistence (n=5–10 cells). (E) ERC1a overexpression rescues the frequency of lamellipodia formation (top) and partially rescues the loss of their persistence (bottom) induced by liprin-α1 silencing. Results are mean±s.e.m. (n=9–17 cells). *P<0.05; **P<0.005 compared with control or as indicated.

GFP-tagged pairs of the components of the complex partially colocalized near the front of migrating cells (supplementary material Fig. S2).

Interestingly, time-lapse images at higher time resolution showed small motile GFP–ERC1a-positive vesicle-like structures appearing near the protruding cell edge, and moving centripetally towards larger dynamic ERC1a-positive structures (supplementary material Movies 3, 4; Fig. 4A–C). The characteristics of these structures suggest that they might be endocytic vesicles. Several exocytic and endocytic markers were tested to identify the dynamic peripheral structures marked by liprin-α1, ERC1a and LL5. A partial colocalization of ERC1a-positive clusters with caveolin, but not with clathrin, was detected in some analyzed cells (Fig. 4D). No colocalization was detected with any other endocytic and Golgi-associated markers tested, nor with functional markers for clathrin-dependent endocytosis, fluid-phase uptake, or clathrin- and dynamin-independent carriers (CLICs) (supplementary material Fig. S3).

Liprin-α1, ERC1a and LL5 proteins are required for the efficient internalization of active β1 integrins

Accumulation of endogenous ERC1a near the leading edge of migrating cells was proximal to, but distinct from, peripheral paxillin-positive focal adhesions (Fig. 5A). The dynamic structures labeled *in vivo* by GFP–ERC1a (Fig. 5B) and GFP–LL5β (supplementary material Movie 5) were often very close to

Journal of Cell Science (2014) 127, 3862–3876 doi:10.1242/jcs.155663

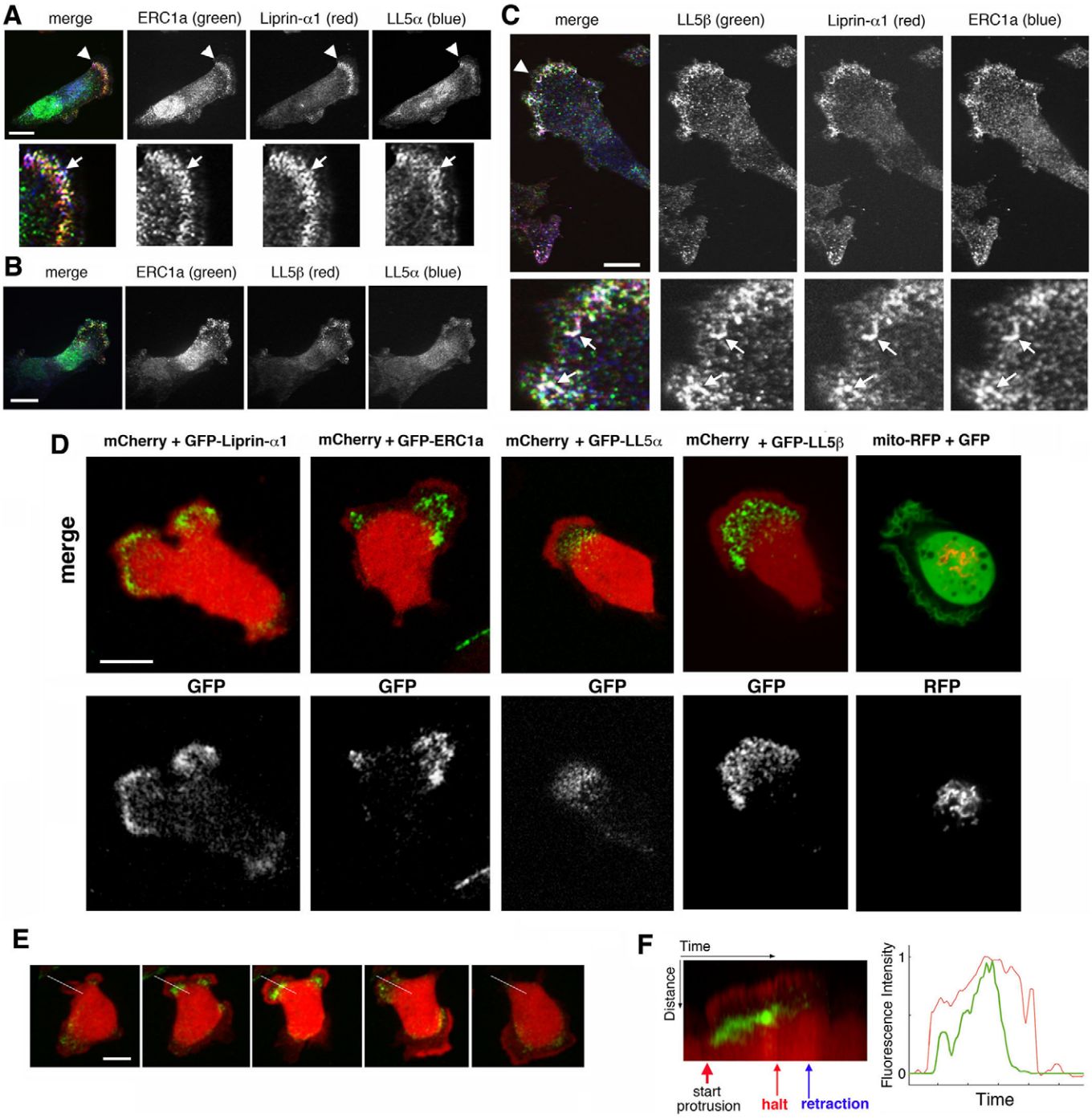

Fig. 3. ERC1a colocalizes with liprin-α1 and LL5β at the edge of migrating cells. MDA-231 cells migrating on fibronectin were immunostained for the endogenous proteins: colocalization at protrusions (arrows) of ERC1a, liprin-α1 and LL5α (A); ERC1a with LL5β and LL5α (B); ERC1a, liprin-α1 and LL5β (C). Scale bars: 10 μm. Lower panels in A and C are threefold enlargements of areas indicated by arrowheads. Arrows indicate examples of colocalization. (D) Frames from cells expressing the indicated proteins and migrating on fibronectin. GFP-tagged liprin-α1, ERC1a, LL5α and LL5β are concentrated in clusters near the leading edge of migrating cells. Cells cotransfected with GFP and Mito-RFP (Mitochondria-RFP) were used as controls. Scale bar: 10 μm. (E) Frames from a time-lapse series of a cell co-transfected with mCherry and GFP–ERC1a. Scale bar: 20 μm. (F) Kymograph for mCherry and GFP–ERC1a from the lamellipodium of the cell shown in E (white line) showing intense accumulation of ERC1a near the lamellipodium during the protrusive phase. The signal for ERC1a decreases abruptly once the lamellipodium halts (red arrow) and retracts (blue arrow). Right, diagram of the intensity of fluorescence for ERC1a (green line) and mCherry (red line). The intensity of ERC1a signal increases soon after lamellipodial protrusion is detectable (red line) and abruptly decreases when the protrusive activity stops.

mCherry–zyxin-positive focal adhesions (Beckerle, 1997), which turn over rapidly at the front of migrating cells. These findings show a tight spatial relationship between the ERC1a- and LL5β-positive structures and dynamic focal adhesions at the protruding front.

There is growing evidence that focal adhesion turnover requires endocytosis and recycling of integrins to and from the cell surface, and that this endocytic cycle is relevant to cell locomotion (Caswell et al., 2009; Valdembri and Serini, 2012).

Journal of Cell Science

Journal of Cell Science (2014) 127, 3862–3876 doi:10.1242/jcs.155663

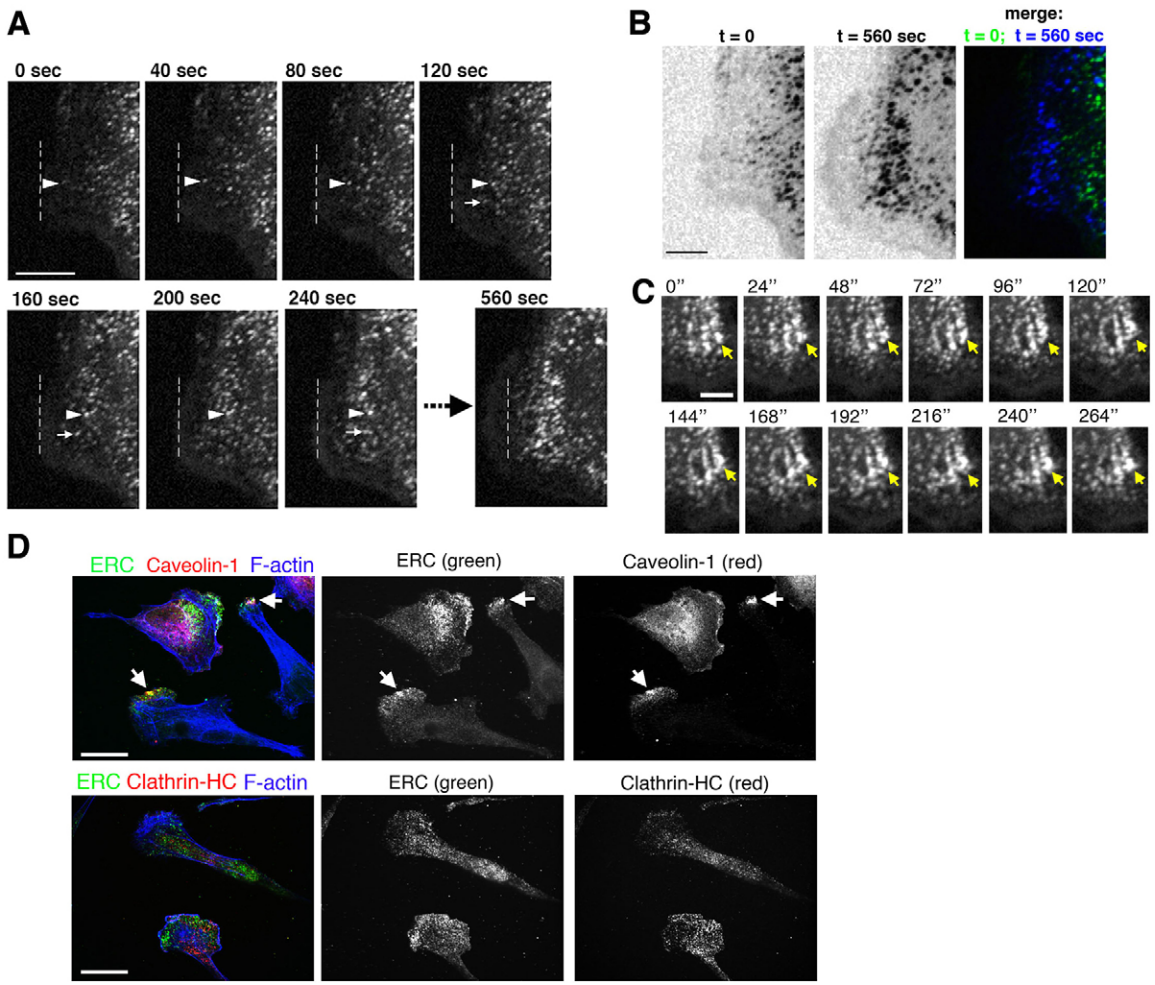

Fig. 4. Dynamic and polarized recruitment of ERC1a near protrusive sites during migration. (A–C) Frames from supplementary material Movie 3 (A,B) and Movie 4 (C). (A) ERC1a-positive vesicle-like structures appear near the protrusive edge. The dashed line in each panel indicates the protruding edge at $t=0$. Arrow and arrowhead show the position of two vesicles moving centripetally from the edge. (B) Inverted images showing the edge of the protruding lamellipodium and the position of the GFP–ERC1a-positive compartment at $t=0$ and $t=560$ s. Merge: color-coded distribution of the GFP–ERC1a-positive compartment at $t=0$ (green) and $t=560$ s (blue). Scale bars: 5 µm. (C) Frames from an ERC1a-positive cluster showing the dynamic nature of the compartment: yellow arrowheads show an example of ERC1a-positive structure with dynamic changes in morphology. Scale bar: 3 µm. (D) ERC1a-positive (ERC) clusters partially colocalize with caveolin-1 at the cell periphery (arrows), whereas no co-staining is observed with clathrin-positive endocytic vesicles detected with antibodies for the heavy chain (HC) of clathrin. Scale bars: 20 µm.

We tested the hypothesis that the liprin-α1, ERC1a and LL5 proteins are involved in integrin endocytosis. Knockdown of either protein did not decrease the density of total β1 integrin at the cell surface detected with the monoclonal antibody (mAb) TS2/16 (Hemler et al., 1984) (Fig. 5C,D); rather, it increased the amount of internalized total β1 integrin after correction for the projected cell area (Fig. 5E,F). We next examined the internalization of active β1 integrin, which accumulates in endocytic compartments (Fig. 6A). Interestingly, depletion of ERC1a, liprin-α1, or LL5 reduced the proportion of internalized active β1 integrin (detected by mAb 9EG7; Lenter et al., 1993) (Fig. 6B,C) by 59.6% (±6.3, s.e.m.) after ERC1a silencing, by 64.8% (±6.5, s.e.m.) after liprin-α1 silencing, and by 40.5% (±8.0, s.e.m.) after LL5 silencing. The decreased internalization of active integrins was not due to a decrease in the density of active integrin β1 at the cell surface, which was indeed increased following ERC1a silencing (Fig. 6D,E). In support of a role of the three proteins in the regulation of integrin traffic, we used an alternative approach that allows the quantification of integrin endocytosis at short times of internalization (Roberts et al., 2001). Biotin-labeled integrins were internalized for 30 min at 37℃ before immunoprecipitation with anti-integrin-β1 antibodies (Fig. 6F). Knockdown of either protein (Fig. 6G) had a negative effect on integrin internalization, with significant decreases measured after liprin-α1 or ERC1a depletion (Fig. 6H).

To test for the specificity of the effects observed on integrin internalization, we looked at the effects of ERC1a depletion on other functional endocytic markers. We used fluorescently labeled transferrin to assess clathrin-mediated endocytosis (supplementary material Fig. S3D,E), fluorescently labeled dextran as a marker of fluid-phase endocytosis (supplementary material Fig. S3F,G), and cholera toxin B as a marker of CLICs (supplementary material Fig. S3H,I). No effects were observed on transferrin and cholera toxin B internalization after silencing ERC1a compared to control cells. ERC1a-depleted cells internalized less dextran, but when the internalization was

Journal of Cell Science (2014) 127, 3862–3876 doi:10.1242/jcs.155663

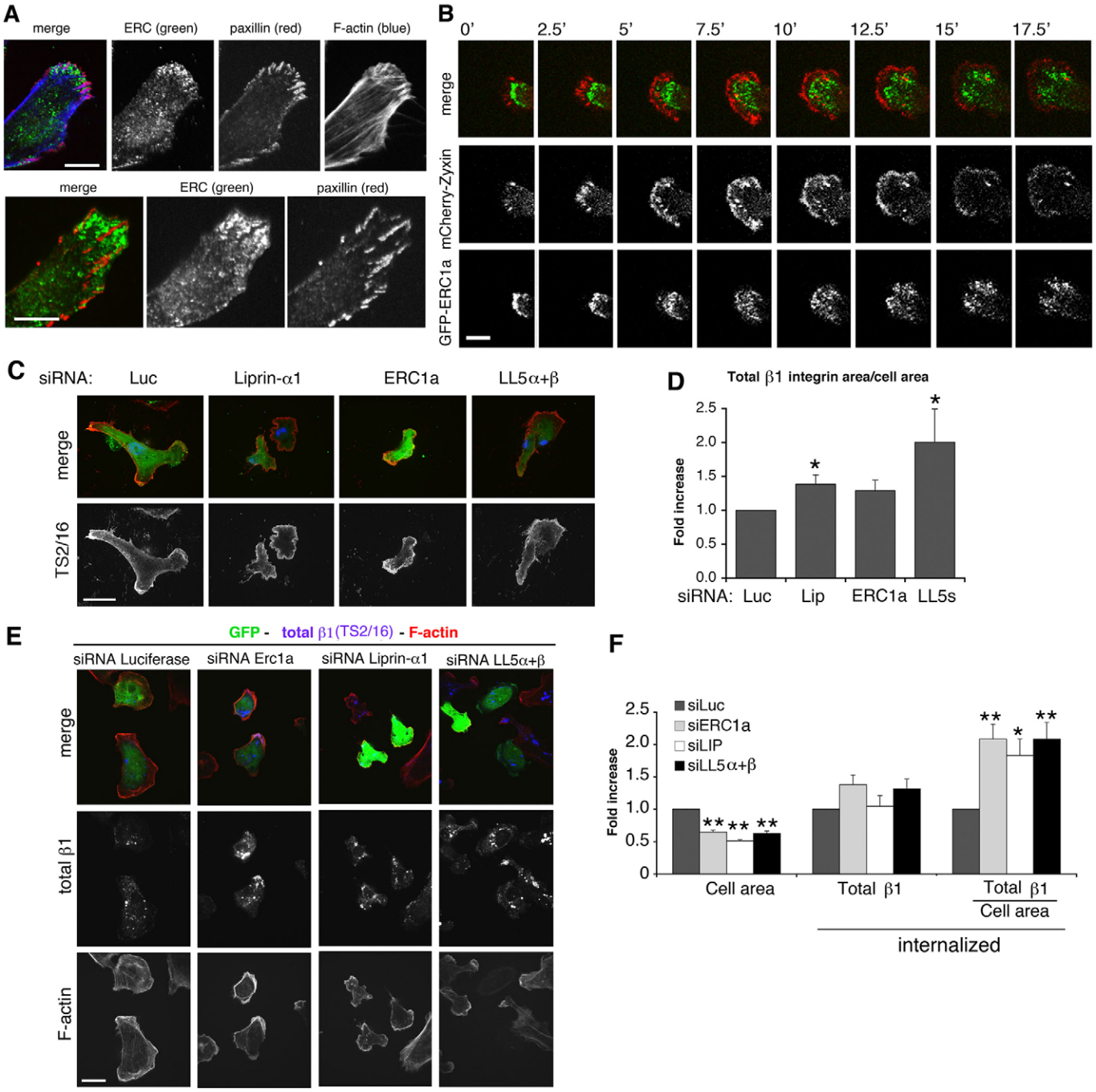

Fig. 5. Silencing of liprin-α1, ERC1a or LL5 proteins enhances the intracellular accumulation of total β1 integrins. (A) ERC1a-positive (ERC) clusters at protrusions are contiguous, but do not overlap, with paxillin-positive focal adhesions. Scale bars: 10 μm. (B) Frames from time-lapse of a cell co-transfected with mCherry–zyxin and GFP–ERC1a. ERC1a accumulates behind peripheral focal adhesions at the front of the migrating cell. Scale bar: 10 μm. (C,D) Cells co-transfected with GFP and the indicated siRNAs (Lip, siLip, liprin-α1; siERC1a, ERC1a; LL5s, siLL5α+β, both LL5α and LL5β) were incubated with the mAb TS2/16 before fixation for immunofluorescence. Merge: GFP (green), integrins (red), DAPI (blue). Results are mean±s.e.m. for the normalized density of β1 integrin at the cell surface (n=36–47 cells). (E,F) Cells transfected with GFP and siRNAs were incubated overnight at 37°C with the TS2/16 mAb. Surface labeling of integrins was removed before fixation and detection of the internalized integrins with fluorescently tagged anti-mouse-IgG antibody. Scale bar: 20 μm (C,E). Silencing of any of the three proteins enhanced total β1 internalization (F). Bars, normalized mean±s.e.m. (n=63–85 cells); *P<0.05; **P<0.005 compared with control.

normalized for the reduced projected cell area induced by ERC1a silencing, no differences were found compared to control cells (supplementary material Fig. S3G).

Given the inhibitory effects observed on cell speed upon depletion of either liprin, ERC or LL5 proteins, these results suggest that liprin-α1, ERC1a and LL5 proteins might promote cell migration by influencing the internalization of active integrins, which are required for adhesion turnover at the cell front. In this direction, we assessed the effects of liprin-α1 depletion on the dynamics of the focal-adhesion-positive edge of

Journal of Cell Science

Journal of Cell Science (2014) 127, 3862–3876 doi:10.1242/jcs.155663

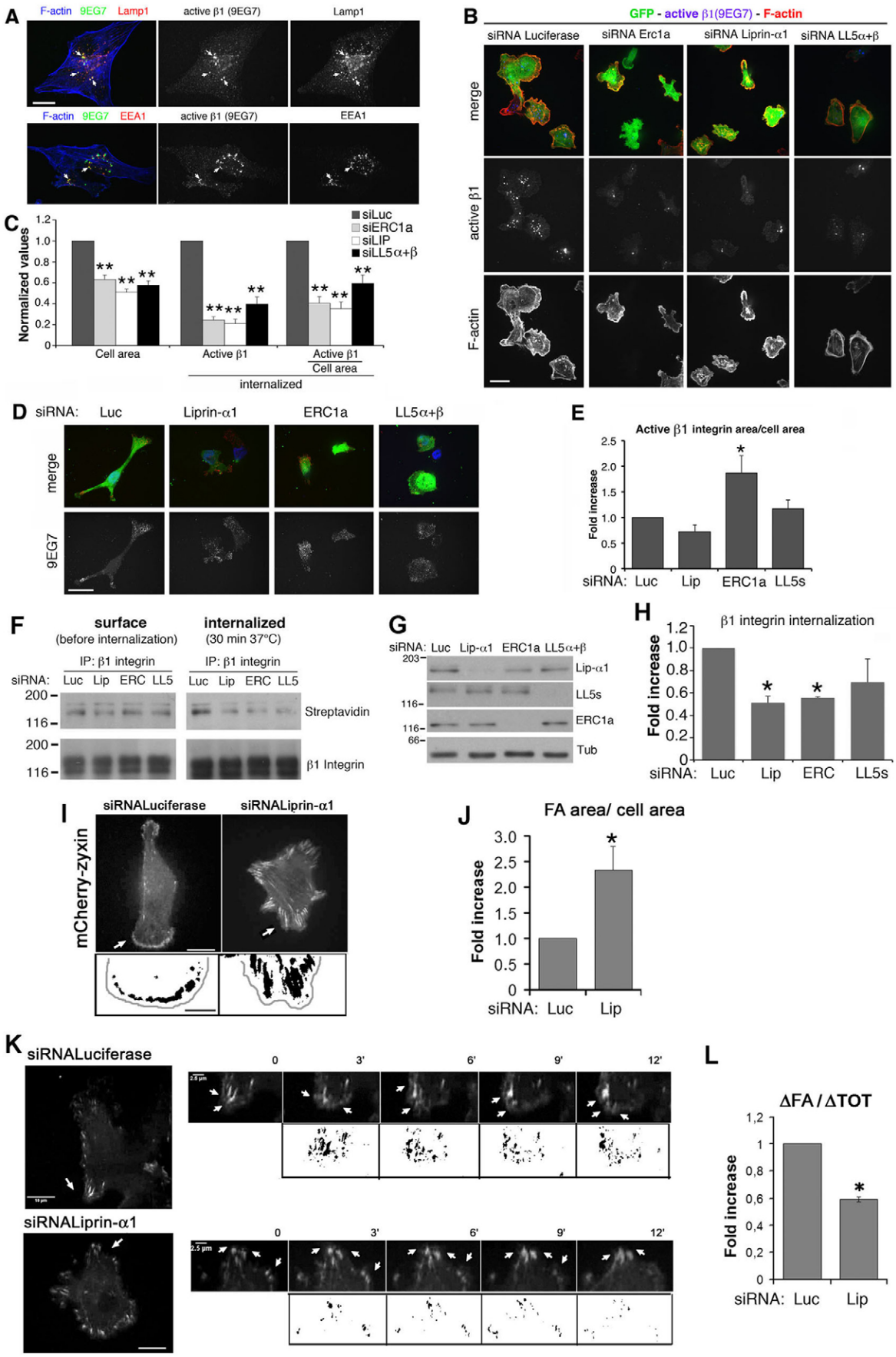

Fig. 6. See next page for legend.

Journal of Cell Science (2014) 127, 3862–3876 doi:10.1242/jcs.155663

Fig. 6. Silencing of liprin-α1, ERC1a or LL5 proteins inhibits the intracellular accumulation of active β1 integrin. (A) Localization of internalized active β1 integrin at endocytic compartments. Cells were incubated overnight with the 9EG7 mAb, surface labeling of β1 integrin was removed before fixation and immunostaining for internalized antibody-bound active β1 integrin receptors and the indicated endocytic markers. Arrows, colocalization of active β1 with late (Lamp1) and early (EEA1) endosomes. Scale bar: 20 μm. (B) Cells co-transfected with GFP and the indicated siRNAs (siLuc, Luc, luciferase; siLip, lip, liprin-α1; ERC, siERC1a, ERC1a; LL5s, siLL5α+β, both LL5α and LL5β) were treated as in A to reveal the internalized active integrins with fluorescently tagged anti-mouse-IgG antibody. (C) Silencing of either protein inhibits active β1 integrin internalization. Results are mean±s.e.m. normalized to control (n=66–80 cells). *P<0.05; **P<0.005 compared with control. (D) Density of active β1 integrin at the plasma membrane. Cells co-transfected with GFP and the indicated siRNAs were incubated with the mAb 9EG7 before fixation and immunofluorescence. Merge: GFP (green), active integrins (red), DAPI (blue). Scale bar: 20 μm. (E) Results are mean±s.e.m. of the normalized density of cell surface integrins (n=36–47 cells). *P<0.05 compared with control. (F) MDA-231 cells transfected with siRNAs were surface labeled with cleavable biotin and lysed immediately (left blot) or after 30 min at 37°C, and removal of the remaining biotin from the cell surface (right blot). Biotin-labeled integrins were immunoprecipitated (IP) with anti-β1 antibodies, and revealed with HRP–streptavidin (upper blots) or with anti-β1 antibodies to reveal total β1 integrin (lower blots). (G) Blots of aliquots of lysates used for the analysis in F, to show silencing of the endogenous proteins by the respective siRNAs. Tub, tubulin. (H) Integrin β1 internalization. Results are mean±s.d. of the normalized integrated densities of bands corresponding to the internalized integrins, corrected for the respective total amount of cell-surface-labeled β1 integrins. *P<0.05 compared with control. (I–L) Liprin-α1 depletion affects the density and turnover of peripheral focal adhesions. MDA-231 cells on fibronectin were co-transfected with mCherry–zyxin and the indicated siRNAs. Density and turnover of adhesions at the cell edge were monitored by confocal imaging. (I) The first frame of a time series of representative mCherry–zyxin-positive cells is shown. Scale bar: 10 μm. The area occupied by focal adhesions at cell protrusions (arrows in upper images) was calculated on thresholded 20-μm×10-μm areas. Cell boundaries are marked by a gray line in the inverted images. Scale bars: 5 μm. (J) Quantification of the area occupied by focal adhesions at the cell margin, normalized to the corresponding total area of the protrusions. Results are means ±s.e.m. (n=14–18 protrusions). *P<0.05 compared with control. (K) Left: low magnification of representative live cells. Scale bars: 10 μm. Right: enlargements showing the protruding areas (arrows in low magnifications) at five different time points; below are the inverted images corresponding to the difference in the area of mCherry–zyxin-positive focal adhesions, between the fluorescence image shown above and the preceding fluorescent frame. Scale bars: 2.5 μm. (L) Quantification of the dynamics of the GFP–zyxin-positive focal adhesion area (ΔFA) divided by the total area of the corresponding protrusion (ΔTOT). See Materials and Methods for details. Results are mean±s.e.m. normalized to control (n=12 protrusions). *P<0.05 compared with control.

migrating cells. We found that silencing of liprin-α1 significantly increased the fraction of projected cell area containing mCherry–zyxin-positive focal adhesions (Fig. 6I,J). Moreover time-lapse on living cells co-transfected with mCherry–zyxin and siRNA against liprin-α1 showed a reduction in the dynamics of the mCherry–zyxin-positive focal adhesion area with respect to cells co-transfected with mCherry–zyxin and control siRNA (Fig. 6K,L).

The PH domain of LL5β is required for efficient cell migration, and for the localization of liprin-α1, ERC1a and LL5 proteins at the cell front

Liprin-α1, ERC1a and LL5β colocalize in a highly polarized and dynamic manner near the protruding edge of migrating cells (Figs 3, 4). We tested whether the accumulation of each protein at sites of protrusion was dependent on the other two proteins. We looked at the subcellular distribution of each endogenous protein after depletion of the other two proteins, and evaluated the accumulation of clusters positive for each protein at protrusions, which were identified as detailed in the Materials and Methods. Analysis by immunoblotting confirmed that single or combined depletion by siRNAs was efficient under all the experimental conditions tested (supplementary material Fig. S4). The subcellular distribution of endogenous ERC1a was strongly affected by depletion of either liprin-α1 or LL5 proteins (the percentage of protrusions per cell containing ERC1a-positive clusters was reduced by 60.1% and 92.2% compared with control, respectively) (Fig. 7A,B). By contrast, the accumulation of LL5β-positive clusters at protrusions was strongly affected by depletion of liprin-α1 (the percentage of protrusions per cell containing LL5β-positive clusters was reduced by 70.6%), but not by ERC1a silencing (Fig. 7C,D). Finally, the accumulation of liprin-α1-positive clusters at protrusions was strongly affected by LL5 depletion but only mildly affected by ERC1a silencing (the percentage of protrusions per cell containing liprin-α1-positive clusters was reduced by 86.9% and 21.9% compared with control, respectively) (Fig. 7E,F). Therefore, although liprin-α1 and LL5β are dependent on each other for their accumulation at protrusions, ERC1a does not play a major role in their localization at these sites. By contrast, the localization of ERC1a depends on both liprin-α1 and LL5 proteins. Depletion of each protein or of pairs of proteins had no or only very mild effects on the number of protrusions per cell (Fig. 7G). This is not surprising because the analysis from time-lapse images showed that lamellipodia could still form in cells silenced for the endogenous proteins, but that they were less stable (Fig. 2A,B). Taken together, these results suggest a functional link between the colocalization of liprin-α1, ERC1a and LL5 at the dynamic polarized structures and the effects of these proteins in stabilizing the protrusive activity during migration. In this regard, depletion of liprin-α1 in cells overexpressing GFP–ERC1a caused the loss of GFP–ERC1a-positive clusters from the cell periphery, as well as the formation of less stable lamellipodia (Fig. 7H), as observed following liprin-α1 depletion in cells with endogenous levels of ERC1a (Fig. 2A,B). A significant increase in the number of focal adhesions was observed in cells overexpressing GFP–ERC1a (Fig. 7I,J). Moreover, ERC1a overexpression induced a faster turnover of the focal adhesions. Both effects required endogenous liprin-α1 because they were inhibited by liprin-α1 silencing (Fig. 7K).

LL5 proteins include a C-terminal PH domain that recognizes phosphatidylinositol-3,4,5-triphosphate (PIP_3), and is required for the subcellular localization of LL5β at the cell cortex (Paranavitane et al., 2003). We investigated the requirement of the PH domain of LL5β for the localization and function of the trimeric complex. Under conditions of low phosphoinositide 3-kinase (PI3K) activity (serum starvation and wortmannin treatment) or upon expression of LL5β with a mutation in the PH domain that prevents binding to PIP3 ($LL5\beta^M$), LL5β predominantly localizes to punctate vesicular structures that are dispersed throughout the cytoplasm (Paranavitane et al., 2007; Takabayashi et al., 2010). The overexpression of the PH mutant $LL5\beta^M$ (Fig. 8A) induced the expected accumulation of the mutant at cytoplasmic vesicles, but did not interfere with the accumulation of endogenous liprin-α1 at the periphery of cells with normal levels of endogenous LL5 proteins (Fig. 8B,D). In addition, the dispersion of liprin-α1 from the peripheral protrusions of LL5-silenced cells (Fig. 7E,F) was rescued by

Journal of Cell Science

Journal of Cell Science (2014) 127, 3862–3876 doi:10.1242/jcs.155663

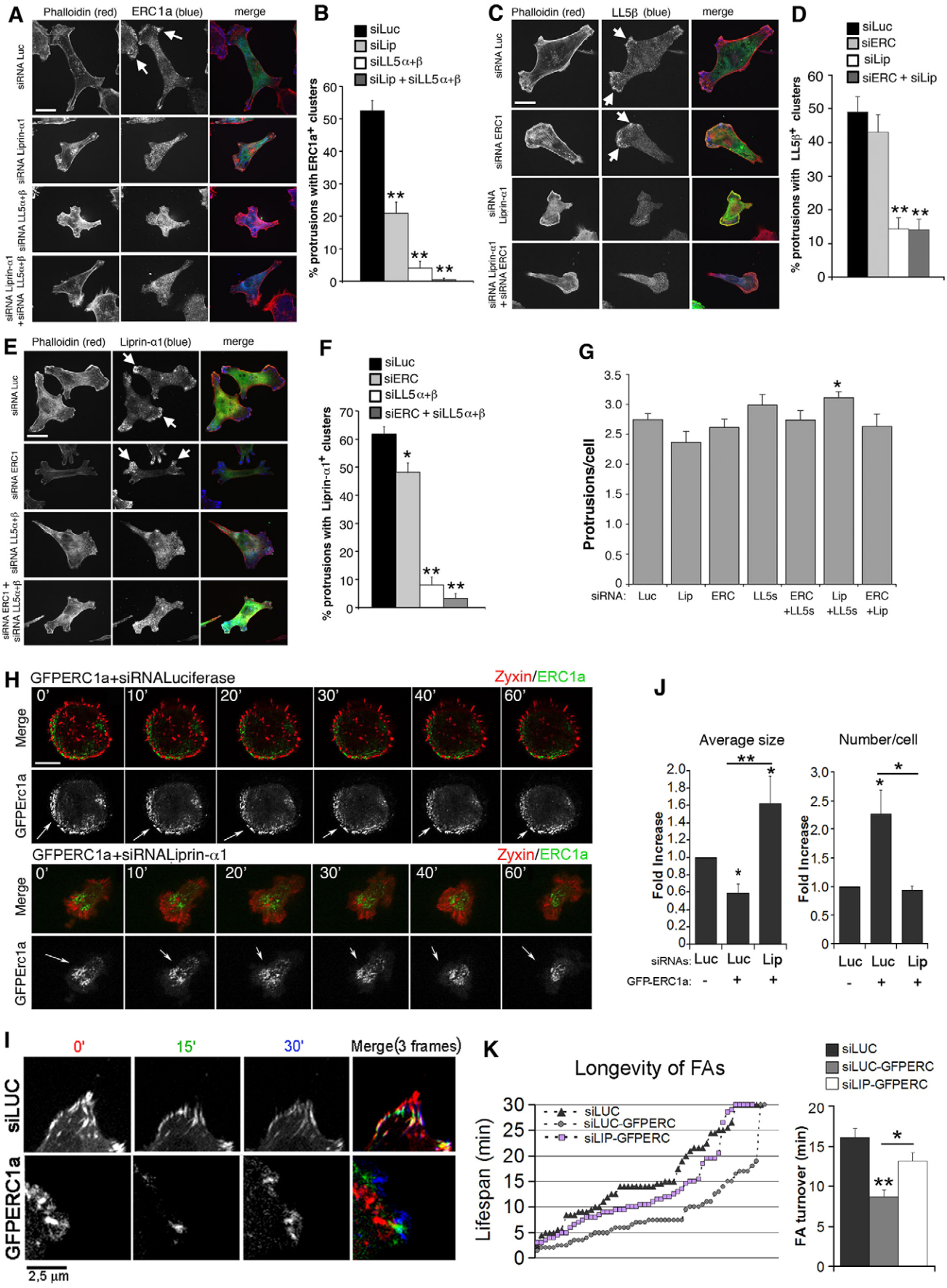

Fig. 7. See next page for legend.

Journal of Cell Science (2014) 127, 3862–3876 doi:10.1242/jcs.155663

Fig. 7. Effects of the depletion of liprin-α1, ERC1a, or LL5 proteins on the subcellular distribution of the remaining endogenous proteins. (A) Distribution of endogenous ERC1a in cells transfected with the indicated siRNAs (siLuc, Luc, luciferase; siLip, Lip, liprin-α1; ERC, siERC, ERC1a; LL5s, siLL5α+β, both LL5α and LL5β). (B) Quantification of the effects of the downregulation of liprin-α1 and/or LL5 on the localization of endogenous ERC1a. Results show the mean±s.e.m. of the percentage of protrusions per cell containing ERC1a-positive clusters (n=54–139 cells). **P<0.005 compared with control. (C) Distribution of endogenous LL5β in cells transfected with siRNAs for control, liprin-α1 and/or ERC1a proteins. (D) Quantification of the effects of the downregulation of ERC1a and liprin-α1 on the subcellular localization of endogenous LL5β. Results represent the mean±s.e.m. of the percentage of protrusions per cell containing LL5β-positive clusters (n=62–80 cells). **P<0.005 compared with control. (E) Distribution of endogenous liprin-α1 in cells transfected with siRNAs for control, ERC1a and/or LL5 proteins. (F) Quantification of the effects of the downregulation of ERC1a and/or LL5 proteins on the localization of endogenous liprin-α1. Results represent the mean±s.e.m. of the percentage of protrusions per cell containing liprin-α1-positive clusters (n=60–161). *P<0.05; **P<0.005 compared with control. In the merge images for A, C and E, F-actin is red, the components of the complex are blue, and GFP (green) is used to identify the cells co-transfected with the indicated siRNAs. Scale bars: 20 μm. (G) Number of protrusions/cell after transfection with siRNAs. (H) Liprin-α1 depletion affects the localization of overexpressed ERC1a at the cell periphery. MDA-231 cells were co-transfected with either GFP or GFP–ERC1a, mCherry–zyxin and the indicated siRNAs. Frames from representative migrating cells are shown. Arrows indicate GFP–ERC1a accumulation in the control cell (top), and after liprin-α1 depletion (bottom). Scale bar: 10 μm. (I) Confocal frames of live MDA-231 cells expressing mCherry–zyxin to label focal adhesions at the cell edge: with (bottom) or without (top) GFP–ERC1a co-expression. The merge of the three color-coded frames shows the turnover of focal adhesions over time. (J) Size (left) and number/cell (right) of mCherry–zyxin-positive focal adhesions. Results are mean±s.e.m. normalized with respect to control cells treated with siRNA against luciferase (left: n=62–378 focal adhesions; right: n=2–5 cells); *P<0.05; **P<0.005 compared with control. (K) Quantification of focal adhesion turnover. The graph on the left displays the average life of single focal adhesions (FAs) (n=53–56) as dots over a period of 30 min. Right graph, dynamic focal adhesion events (assembly and disassembly) during 30 min. Results are persistence mean±s.e.m., determined as the average number of zyxin-positive dots appearing or disappearing per min at cell protrusions; n=53–56 focal adhesions. *P<0.05; **P<0.005 compared with control.

the expression of siRNA-resistant GFP-tagged mouse wild-type LL5β, but not by the expression of the LL5β^M PH mutant (Fig. 8C,D): endogenous liprin-α1 remained mainly diffuse localized throughout the cytoplasm and did not colocalize with the GFP–LL5β^M-positive dots induced by the mutant (Fig. 8C). The expression of GFP–LL5β^M either in cells with endogenous LL5 (Fig. 8E) or after silencing LL5 (Fig. 8F) caused the recruitment of endogenous ERC1a to the GFP–LL5β^M-positive dots, probably owing to the interaction of ERC1a with LL5β^M (supplementary material Fig. S1D). These results indicate that the PH domain of LL5β is required for the accumulation of the trimeric complex near the protrusions. However, the presence of the PH domain is not sufficient for the recruitment of the complex, because our data in Fig. 7 indicate the additional requirement of liprin-α1 for the accumulation of the complex at the protrusions.

The silencing of LL5 proteins causes a defect in migration (Fig. 1) and in lamellipodial dynamics (Fig. 2). The defect in migration was rescued by the expression of the GFP-tagged wild-type LL5β protein, but not by the GFP–LL5β^M PH mutant (Fig. 8G). Analysis of lamellipodial dynamics demonstrated that the defect induced by LL5 silencing was fully rescued by the wild-type GFP–LL5β, and only partially rescued by GFP–LL5β^M, given that a significant defect in lamellipodial persistence was still observed in cells expressing the PH mutant (Fig. 8H,I). Taken together, these results show that the PH domain of LL5β is required for the proper localization of liprin-α1 and ERC1 at the cell edge, and support the hypothesis that there is a functional link between the subcellular accumulation of the three proteins to the protrusions and their requirement for the stability of the lamellipodia and efficient migration.

DISCUSSION

Our results show that liprin-α1, ERC1a and LL5 proteins cooperate to drive efficient migration on and through ECM. They do so by stabilizing the lamellipodia at the front of migrating cells, where the three proteins partially colocalize in newly identified dynamic cytoplasmic structures that are highly polarized and specifically concentrated near the active protrusions. The effects of the silencing of any of the three proteins on the stability of the lamellipodia and their subcellular colocalization indicate that they are part of the same functional network. The negative effects of the silencing of any of the proteins on the lamellipodial stability in 2D and 3D environments might explain the consistent defects observed in the migration and invasion of the silenced cells.

Liprin-α1, ERC1/ELKS and LL5β have previously been shown to colocalize at cortical platforms at the periphery of non-motile cells, where these proteins are required to stabilize microtubules through CLASP proteins. These sites displayed no significant motility, behaving as stable and relatively immobile structures at the periphery of HeLa cells (Lansbergen et al., 2006; van der Vaart et al., 2013). In contrast, the structures identified by the three proteins in actively migrating MDA-231 are highly dynamic and concentrated to restricted areas of the cell corresponding to active protrusions, where they partially colocalize with caveolin.

ERC proteins have been implicated in membrane trafficking: ERC2 and liprin-α regulate presynaptic vesicle traffic in neurons (Dai et al., 2006); in non-neuronal cells ERC1 participates in the docking and/or fusion of Rab6-positive vesicles at the cell cortex and, together with liprin-α, in secretion in mast cells (Grigoriev et al., 2007; Nomura et al., 2011). Here, we observed a strong and specific inhibition of the internalization of active β1 integrin after depletion of ERC1a, liprin-α1 or LL5 proteins, whereas other endocytic pathways were not affected. Based on these results and on the identification of ERC1a-positive dynamic vesicle-like structures by video microscopy, we speculate that the identified cytoplasmic structures represent a functional state of an endocytic compartment characterized by the recruitment of ERC, LL5 and liprin-α1 on the cytoplasmic side of intracellular membranes.

The localization of LL5β at the cell membrane is dependent on PIP_3 (Paranavitane et al., 2003). Mutation of the LL5β PH domain perturbs the accumulation of the other proteins of the complex at the cell periphery, and negatively affects lamellipodial stability and cell motility. Based on these results and on the observed negative effects of the depletion of each component on the localization of the remaining proteins, and on the tight association of liprin-α1 to the cytoplasmic side of the plasma membrane (Asperti et al., 2009; Asperti et al., 2010), we propose a model in which liprin-α1 and LL5β are recruited with ERC1a to the cytoplasmic side of the plasma membrane and, eventually, to the cytoplasmic side of endocytic vesicles during cell migration (Fig. 8J). This mechanism might be relevant to the turnover of adhesions observed at the front of highly motile cells.

Journal of Cell Science (2014) 127, 3862–3876 doi:10.1242/jcs.155663

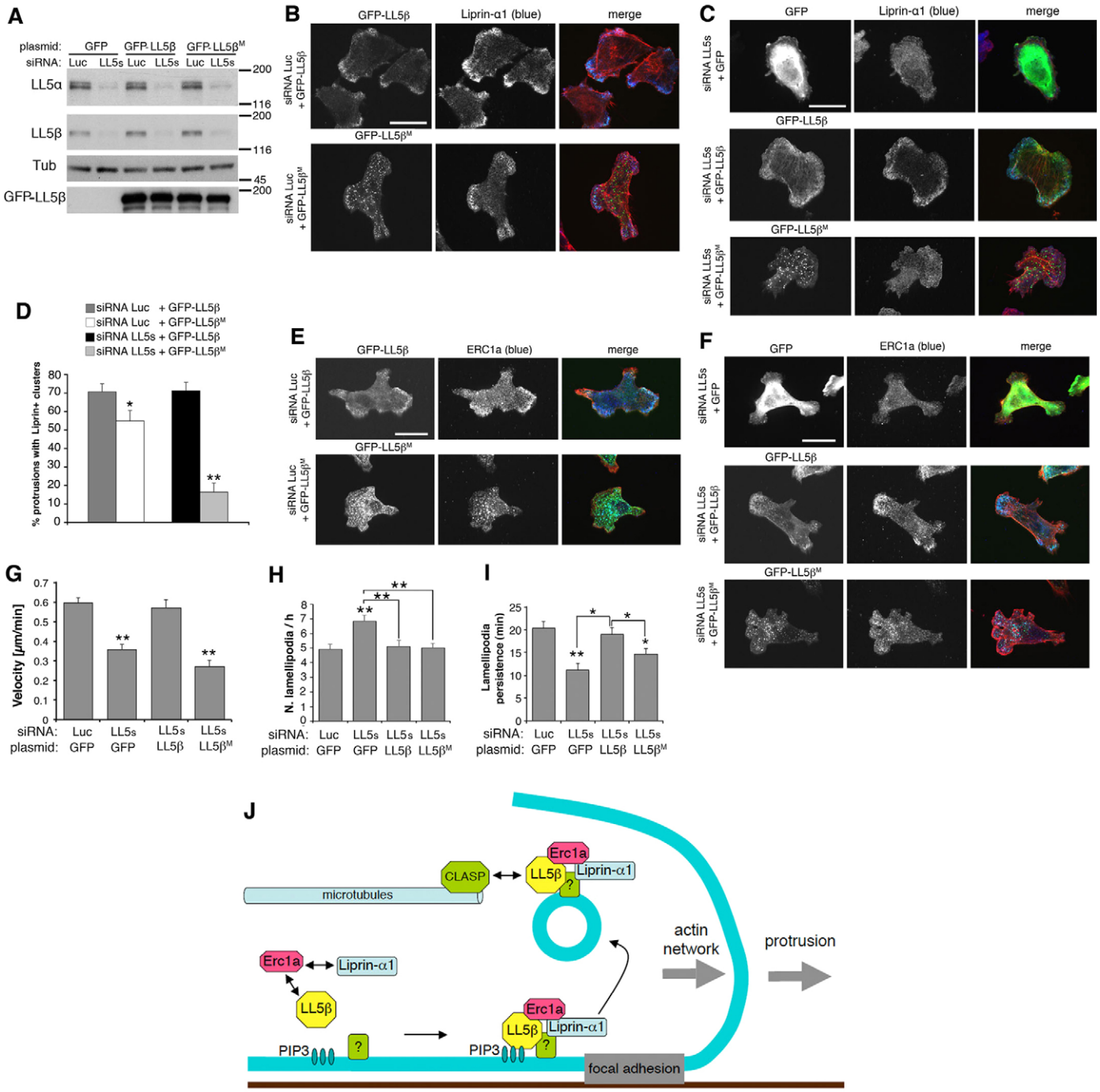

Fig. 8. The PH domain of LL5β is required for effective migration, and for the localization of endogenous liprin-α1 and ERC1a near the protruding cell edge. (A) siRNAs specific for endogenous LL5 proteins (LL5s) (upper two blots from top) do not interfere with the expression of GFP-tagged mouse wild-type and mutant LL5β (lowest blot). Immunoblotting was performed on lysates (15 μg protein) from transfected cells to detect the proteins indicated on the left of each blot. The anti-LL5β antibody recognizes the endogenous human protein, but not the murine overexpressed protein. Luc, luciferase. (B,C) Subcellular localization of endogenous liprin-α1 in cells co-transfected with siRNAs for either control or LL5 proteins, together with the indicated GFP constructs. Scale bars: 20 μm. (D) Effects of the expression of wild-type LL5β or the mutant LL5β^M on the accumulation of endogenous liprin-α1 at the cell edge. Results are mean±s.e.m. (n=45–76 cells). *P<0.05; **P<0.005 compared with control. (E,F) Localization of endogenous ERC1a in cells co-transfected with siRNAs for either control or LL5 proteins, together with the indicated GFP constructs. Scale bars: 20 μm. (G) The negative effects of LL5 proteins depletion on the speed of migration on fibronectin are rescued by GFP–LL5β, but not by GFP–LL5β^M. Results are mean±s.e.m. (n=42–81 cells). The effects of LL5 proteins depletion on the formation (H) and the persistence (I) of lamellipodia during migration on fibronectin are rescued by the wild-type GFP–LL5β. The GFP–LL5β^M mutant can rescue the formation (H), and only partially rescue the persistence (I), of lamellipodia. Results are means ±s.e.m. (n=11–17 cells). *P<0.05; **P<0.005 compared with control or as indicated. (J) Model for the functional interactions of the liprin-α1, ERC1a and LL5 proteins. See text for details.

Journal of Cell Science (2014) 127, 3862–3876 doi:10.1242/jcs.155663

In this regard, in actively migrating cells, the three proteins colocalize dynamically, close to the centripetal side of the focal adhesions at the protruding edge, more distal from the plasma membrane. The rapid dynamics of focal adhesion at these sites is expected to require fast active integrin turnover. There is growing evidence that internalized integrins can be rapidly recycled at the front of migrating cells: localized endocytic and exocytic traffic of integrins can spatially restrict receptor distribution to promote the turnover of adhesions and signaling molecules at the cell front and to support protrusion (Caswell et al., 2009). It is known that β1 integrin can be internalized (Pellinen et al., 2008; Shi and Sottile, 2008) in both inactive and ligand-bound active conformations (Ng et al., 1999; Valdembri et al., 2009; Dozynkiewicz et al., 2012), and that the two pools might be recycled through distinct routes (Arjonen et al., 2012). The negative effect of the lack of liprin-α1, ERC1a or LL5 on the specific internalization of active β1 integrin supports the hypothesis that the dynamic structures identified in this study are directly or indirectly involved in the internalization of integrins, thus contributing to the turnover of focal adhesions at the front of migrating cells. Although a clear accumulation of β1 integrin in the peripheral ERC1a-positive structures could not be detected (our unpublished data), a rapid and transient association of the internalized receptors with the proposed ERC1a-positive structures cannot be excluded. Interestingly, in polarized epithelial cells, LL5 proteins colocalize with laminin-5 and its integrin receptors α3β1 and α6β4 at the basal side, possibly owing to indirect interaction of LL5 with the cytoplasmic tails of the α-integrin subunits (Hotta et al., 2010).

In conclusion, we would like to propose that the highly polarized and dynamic structures specified by liprin-α1, ERC1a and LL5 proteins identify a new mechanism that is important for lamellipodia stabilization and adhesion turnover, both of which are required for efficient protrusion during migration.

MATERIALS AND METHODS

Plasmids

Plasmids for FLAG–liprin-α1 and GFP–liprin-α1 (human), GFP–LL5α (human), GFP–LL5β (mouse), GFP–ERC1a (full-length murine ELKSε), mCherry–zyxin, and Mito-RFP were as described previously (Totaro et al., 2007; Asperti et al., 2009; Hotta et al., 2010; Kishi et al., 2005; Inoue et al., 2006; Colombelli et al., 2009). GFP–LL5β^{M} was generated by PCR with primers 5′-GGTGGGAAAATTAAAACGTGGAAAGCA-GCCTGGTTTGTTTTTGACCGGAATAAG-3′ and 5′-CTTATTCCGG-TCAAAAACAAACCAGGCTGCTTTCCACGTTTTAATTTTCCC-ACC-3′ to give two mutations (K1211A, R1212A) in the PH domain of murine LL5β (accession number NP_001239371.1). The mCherry–liprin-α1, mCherry–ERC1a and mCherry-C1–LL5β were generated from plasmids for the corresponding GFP-tagged proteins. The pEGFP-Liprin-α1^{SR} plasmid was obtained by site-direct mutagenesis on pEGFP-Liprin-α1 (primers: 5′-TTAACCCAGGGGAAGTTACACGAAGTGGGTCAC-GAAAGAGATTCCTTGCAGAGACAGCTC-3′ and 5′-GAGCTGTCT-CTGCAAGGAATC TCTTTCGTGACCCACTTCGTGTAACTTCCCC-TGGGTTAA-3′).

Antibodies and endocytic markers

The polyclonal antibody (pAb) against liprin-α1 was as described previously (Asperti et al., 2009); the commercial mAb against liprin-α1 was from Proteintech. The mAb for both LL5α and LL5β (clone IH12), the hamster mAb against LL5α (223), and pAb against mannose 6-phosphate receptor were as described previously (Ludwig et al., 1991; Hotta et al., 2010; Kishi et al., 2005). Other mAbs were specific for: Golgi 58K, ERC1a (ELKS-30), Lamp1 (H4A3) from Abcam; EEA1, 9EG7 specific for active β1 integrins, paxillin (349) and GM130 (35) from BD Biosciences; Rab6 (D37C7) from Cell Signaling; TS2/16, recognizing the extracellular portion of β1 integrin, from American Type Culture Collection; tubulin-α (Clone DM 1A) from Sigma; clathrin heavy chain (TD.1) from Santa Cruz Biotechnology. The β1 integrin pAb used for immunoprecipitation was as described previously (Tomaselli et al., 1988). Commercial pAbs specific for GFP (Life Technologies), fibronectin and LL5β (Sigma); caveolin-1 (N-20), giantin (H-49), paxillin (H-114) (Santa Cruz Biotechnology); GFP (chicken pAb; Abcam). FITC- and TRITC-Phalloidin were from Sigma. Alexa-Fluor-conjugated secondary antibodies, dextran–Alexa-Fluor-568, transferrin–Alexa-Fluor-647, CtxB (cholera toxin B)–Alexa-Fluor-555 and horseradish peroxidase (HRP)-conjugated streptavidin were from Life Technologies. EZ-link cleavable sulfo-NHS-SS-biotin (#21331) was from Thermo Scientific; MesNa (sodium 2-mercaptoethanesulfonate, #63705) was from Fluka, and iodoacetamide from Sigma.

Transfection and isolation of cell lines with stable expression of GFP-Liprin-α1

Cells were transfected with Lipofectamine-2000® (Life Technologies) with 1–2 μg of plasmid and/or 50–100 nM of siRNAs, and used 24–48 h later. siRNAs (Life Technologies) for luciferase, liprin-α1, ERC1a, LL5β and LL5α were as described previously (Asperti et al., 2009; Lansbergen et al., 2006; Ducut Sigala et al., 2004; Hotta et al., 2010; Astro et al., 2011). The region targeted by siRNA for human LL5β includes two mismatches with respect to the mouse cDNA sequence, making this latter resistant to silencing. Second siRNAs for human LL5α (5′-GATGGGT-TAGCCACCCGTA-3′) and LL5β (5′-GGATCTACCTCATAGCGTA-3′) were from Qiagen.

Cell lines stably expressing either GFP–liprin-α1 or GFP were obtained after transfection of MDA-231 cells with 2 μg of either GFP–liprin-α1 or GFP plasmid, respectively. Clones resistant to 1 mg/ml of G418 (Merck Millipore) were expanded from single cells isolated by limiting dilution.

Biochemical analysis

Immunoprecipitates from cell lysates incubated with Protein-A–Sepharose beads (Amersham Biosciences) conjugated to antibodies, were separated by SDS-PAGE for immunoblotting.

Viability and proliferation assay

Cell viability was assessed by a colorimetric assay based on the reduction of MTT [3-(4,5-dimethylthiazol-2yl)-2,5-diphenyl-tetrazolium bromide]. For cell proliferation, 2000 cells were seeded in 24-well plates and their growth was evaluated by counting in Burker chamber every 24 h.

Motility assays

Haptotactic migration, cell spreading, and invasion assays were as described previously (Astro et al., 2011). Data were normalized to control and presented as means±s.e.m. For random migration, transfected cells seeded for 2 h at 37℃ on 2.5 μg/ml fibronectin (50,000 cells per 3.5-cm diameter well) were imaged for 5 h at 6-min intervals with an Axiovert microscope (Zeiss) equipped with an Orca II CCD camera (Hamamatsu), and analyzed with ImageJ (NIH). For lamellipodial dynamics, frames were analyzed with ImageJ by counting the number of lamellipodia forming during 1 or 5 h. Persistence of protrusions was evaluated as the time elapsed between the formation of a lamellipodium and its disassembly. Statistically significant differences were analyzed Student's *t*-test.

Migration in reconstituted ECMs

3D matrices were prepared as described previously (Cukierman et al., 2001; Cukierman, 2005). Transfected MDA-231 cells were seeded on matrices for 6 h before microscopy. Frames were acquired every 7 min for 8 h, and analyzed with ImageJ.

Morphological analysis

MDA-231 cells (10^5 cells) in fibronectin-coated (2.5 μg/ml) coverlips were transfected after 1 day, and used for video imaging or immunofluorescence 24–48 h later (Astro et al., 2011). Live imaging was performed on Inverted Eclipse TE2000-E microscope (Nikon) with a

spinning-disc head (CSU-10, Yokogawa) equipped with a Cool SNAP HQ2 CCD camera (Photometrics). Pictures were at 1 frame/min or 0.5 frames/s. Images of fixed cells were acquired with a confocal Ultraview ERS system from PerkinElmer.

The quantification of the accumulation of clusters positive for liprin-α1, ERC1a and/or LL5 proteins at protrusions was performed as follows: we considered as protrusions the cellular extensions that showed a clear F-actin-positive edge. We counted the number of protrusions with protein-positive clusters and the number of total protrusions in each cell. We calculated the ratio between these two values (number of protrusions with protein-positive clusters/number of total protrusions). Average ratios from several cells for each experimental condition are expressed as percentages; the numbers of cells considered for each condition are indicated in the respective figure legends.

Integrin-β1–antibody internalization assay

Transfected MDA-231 cells on fibronectin-coated (2.5 µg/ml) coverslips were incubated overnight at 37℃, under 5% CO_2 in growth medium with either 2 µg/ml TS2/16 mAb, or 1.25 µg/ml 9EG7 mAb (Margadant et al., 2012). Cell-surface-bound antibodies were stripped with 0.5 M NaCl and 0.5% acetic acid, pH 2. After fixation and permeabilization with 0.1% saponin, cells were immunostained with Alexa-Fluor-conjugated secondary antibodies. Quantification of internalized integrin–antibody complexes was performed with ImageJ. For quantitative analysis, exposure time, gain and offset were adjusted to avoid saturated pixels. Images were acquired at the same exposure and identically thresholded integrin images were used to measure the area occupied by internalized integrins (positive for 9EG7 or TS2/16). The projected cell area was measured on thresholded GFP images. Values obtained are represented as fold increase compared to control cells (siRNA against luciferase) of: (1) the projected cell area; (2) the area occupied by internalized integrins; and (3) the fraction of the cell area occupied by internalized integrins. Data were from two or three experiments in which at least 60 cells were analyzed.

Biotin–integrin-β1 internalization assay

We used a modification of the biochemical method described previously to quantify integrin internalization at shorter times, based on the immunoprecipitation of biotinylated integrins (Roberts et al., 2001). MDA-231 cells transfected with siRNAs were cooled on ice, rinsed twice with PBS and exposed for 30 min at 4℃ to 0.5 mg/ml EZ-link cleavable sulfo-NHS-SS-biotin (Thermo Scientific) in Hank's balanced salt solution (Life Technologies). After removing unbound biotin with cold medium, the cells were either lysed immediately to identify the surface receptor pool, or incubated for 30 min at 37℃ to allow the internalization of integrins. Cells were then washed twice with cold PBS, and the remaining biotin-labeled surface proteins removed by a 45-min incubation at 4℃ in 60 mM sodium 2-mercaptoethanesulfonate (MesNA), 100 mM NaCl, 50 mM Tris-HCl pH 8.6, followed by quenching for 15 min on ice with 100 mM iodoacetamide (Sigma). The cells were lysed, and biotinylated integrins were immunoprecipitated with anti-integrin-β1 pAb (Tomaselli et al., 1988) conjugated to protein-A–sepharose beads. As control of protein biotinylation, one dish was lysed after labeling, without treatment with MesNA. Lysates and immmunoprecipitates of internalized or surface biotinylated integrins were detected with HRP-conjugated streptavidin (Life Technologies). Blots were then stripped in acid buffer (0.2 M glycine, 0.1% SDS, 1% Tween-20, pH 2.2) and re-probed with anti-β1-integrin pAb. Biotinylated surface and intracellular β1 integrins were quantified with ImageJ from bands of immunoprecipitates. The relative amount of internalized biotin-labeled integrin were normalized to the corresponding amounts of total biotin-labeled surface integrin (before internalization). Data are expressed as fold increase compared to control cells (siRNA against luciferase) of the integrated density of the bands from blots, from two independent experiments.

Analysis of focal adhesion density and turnover

MDA-231 cells seeded on 24-mm diameter glass coverlips precoated with 2.5 µg/ml fibronectin (120,000 cells/well) were co-transfected with siRNAs and mCherry–zyxin. Confocal live imaging was performed 48 h later on an inverted spinning-disc Ultraview ERS confocal microscope (PerkinElmer) equipped with a temperature- and CO_2-controlled stage. Images were acquired with a 100× 1.3 NA oil immersion objective (Zeiss) for 30 min at 0.5 frames/min. Identical exposure and laser power were used for all samples. Pictures were taken at the same exposure with a 532-nm laser. Quantitative analysis of focal adhesion density and turnover was performed with ImageJ on thresholded mCherry–zyxin images. The same threshold was used for all conditions within a single experiment. Quantification of focal adhesion density at the cell edge was performed on the first image of each time series. Areas of 20-µm×10-µm were positioned on protrusions to measure the area of peripheral adhesions. Values were expressed as fractions of marginal cell area occupied by adhesions, and were normalized to the values obtained for control cells (siRNA against luciferase). Data were collected from 14–18 active cell protrusions from two or three independent experiments.

For the quantification of adhesions turnover, we used a modification of a published protocol (Grande-García et al., 2007). We measured the changes in mCherry–zyxin-positive area at the periphery of migrating cells on thresholded images collected over 30 min, by applying the operation 'difference' of the 'image calculator' function of ImageJ. We obtained 15 'subtracted' consecutive frames for each protrusion. The measure of the differences between mCherry–zyxin-positive areas from consecutive frames was defined as ΔFA. From the same 15 subtracted consecutive frames we calculated, in parallel, the changes of the corresponding total area occupied by the protrusion (ΔTOT). The ratio between the ΔFA and ΔTOT values represents a measure of adhesion turnover. These values were normalized to control cells (siRNA Luciferase). Data were from 12 active cell protrusions per conditions, from two or three independent experiments.

For the analysis in cells overexpressing GFP–ERC1a, number and size of mCherry–Zyxin-positive focal adhesions were quantified on thresholded images by the Analize Particles plugin of ImageJ (version 1.48t). Values were represented as fold increase compared with control cells. For quantification of focal adhesion turnover, time of formation and disappearance of each adhesion from protruding areas was monitored, and lifetimes were determined for each condition. Each experiment was repeated at least two times.

Dextran, transferrin and CtxB uptake

Uptake of endocytic markers was performed as described previously (Howes et al., 2010, Fletcher et al., 2012). Briefly, 48 h after transfection cells on fibronectin were incubated for 30 min at 37℃ with 1 mg/ml dextran–Alexa-Fluor-568, 20 µg/ml transferrin–Alexa-Fluor-647 or 10 µg/ml CTxB–Alexa-Fluor-555 (Hewlett et al., 1994). After washing and removal of surface-bound transferrin by 0.5 M glycine, pH 2.2, cells were fixed with 3% parafolmaldehyde for confocal analysis.

Acknowledgements

We thank Joshua R. Sanes (Harvard University, Cambridge, MA) for LL5 mAb and GFP–LL5β, Yuko Mimori-Kiyosue (Kobe Institute, Japan) for LL5α mAb and GFP–LL5α, Yoshimi Takai (Osaka University, Japan) for GFP–ERC1a, Vic Small (Institute of Molecular Biotechnology, Vienna, Austria) for mCherry–zyxin, and Bernard Hoflack (Dresden University of Technology, Dresden, Germany) for the mannose-6-phosphate receptor pAb. We thank Francesca Capriotti, Diletta Tonoli, Cesare Covino (Alembic) for technical help, and Jacopo Meldolesi (San Raffaele Scientific Institute, Milano, Italy) for critical reading of the manuscript.

Competing interests

The authors declare no competing interests.

Author contributions

Experiments were designed by V.A., I.d.C. and M.F., and were performed by V.A., S.C. and E.M.. Some time-lapse imaging series were performed in the laboratory of M.F. I.d.C., with the help of V.A., wrote the manuscript.

Funding

This study was supported by grants from Associazione Italiana per la Ricerca sul Cancro (AIRC) [grant number IG 10321 to I.d.C.]; Telethon Foundation Italy [grant number GGP12126 to I.d.C.]; and the Italian Ministry for Research [grant number

PRIN 20108MXN2J to I.d.C.]. V.A. is the recipient of a fellowship from Fondazione Italiana per la Ricerca sul Cancro (FIRC).

Supplementary material

Supplementary material available online at
http://jcs.biologists.org/lookup/suppl/doi:10.1242/jcs.155663/-/DC1

References

Arjonen, A., Alanko, J., Veltel, S. and Ivaska, J. (2012). Distinct recycling of active and inactive β1 integrins. *Traffic* **13**, 610-625.

Asperti, C., Astro, V., Totaro, A., Paris, S. and de Curtis, I. (2009). Liprin-alpha1 promotes cell spreading on the extracellular matrix by affecting the distribution of activated integrins. *J. Cell Sci.* **122**, 3225-3232.

Asperti, C., Pettinato, E. and de Curtis, I. (2010). Liprin-alpha1 affects the distribution of low-affinity beta1 integrins and stabilizes their permanence at the cell surface. *Exp. Cell Res.* **316**, 915-926.

Astro, V., Asperti, C., Cangi, M. G., Doglioni, C. and de Curtis, I. (2011). Liprin-α1 regulates breast cancer cell invasion by affecting cell motility, invadopodia and extracellular matrix degradation. *Oncogene* **30**, 1841-1849.

Beckerle, M. C. (1997). Zyxin: zinc fingers at sites of cell adhesion. *Bioessays* **19**, 949-957.

Caswell, P. T., Vadrevu, S. and Norman, J. C. (2009). Integrins: masters and slaves of endocytic transport. *Nat. Rev. Mol. Cell Biol.* **10**, 843-853.

Colombelli, J., Besser, A., Kress, H., Reynaud, E. G., Girard, P., Caussinus, E., Haselmann, U., Small, J. V., Schwarz, U. S. and Stelzer, E. H. (2009). Mechanosensing in actin stress fibers revealed by a close correlation between force and protein localization. *J. Cell Sci.* **122**, 1665-1679.

Cukierman, E. (2005). Cell migration analyses within fibroblast-derived 3-D matrices. *Methods Mol. Biol.* **294**, 79-93.

Cukierman, E., Pankov, R., Stevens, D. R. and Yamada, K. M. (2001). Taking cell-matrix adhesions to the third dimension. *Science* **294**, 1708-1712.

Dai, Y., Taru, H., Deken, S. L., Grill, B., Ackley, B., Nonet, M. L. and Jin, Y. (2006). SYD-2 Liprin-alpha organizes presynaptic active zone formation through ELKS. *Nat. Neurosci.* **9**, 1479-1487.

de Curtis, I. (2011). Function of liprins in cell motility. *Exp. Cell Res.* **317**, 1-8.

de Curtis, I. and Meldolesi, J. (2012). Cell surface dynamics – how Rho GTPases orchestrate the interplay between the plasma membrane and the cortical cytoskeleton. *J. Cell Sci.* **125**, 4435-4444.

Deguchi-Tawarada, M., Inoue, E., Takao-Rikitsu, E., Inoue, M., Ohtsuka, T. and Takai, Y. (2004). CAST2: identification and characterization of a protein structurally related to the presynaptic cytomatrix protein CAST. *Genes Cells* **9**, 15-23.

Dozynkiewicz, M. A., Jamieson, N. B., Macpherson, I., Grindlay, J., van den Berghe, P. V., von Thun, A., Morton, J. P., Gourley, C., Timpson, P., Nixon, C. et al. (2012). Rab25 and CLIC3 collaborate to promote integrin recycling from late endosomes/lysosomes and drive cancer progression. *Dev. Cell* **22**, 131-145.

Ducut Sigala, J. L., Bottero, V., Young, D. B., Shevchenko, A., Mercurio, F. and Verma, I. M. (2004). Activation of transcription factor NF-kappaB requires ELKS, an IkappaB kinase regulatory subunit. *Science* **304**, 1963-1967.

Fletcher, S. J., Poulter, N. S., Haining, E. J. and Rappoport, J. Z. (2012). Clathrin-mediated endocytosis regulates occludin, and not focal adhesion, distribution during epithelial wound healing. *Biol. Cell* **104**, 238-256.

Gauthier, N. C., Masters, T. A. and Sheetz, M. P. (2012). Mechanical feedback between membrane tension and dynamics. *Trends Cell Biol.* **22**, 527-535.

Grande-García, A., Echarri, A., de Rooij, J., Alderson, N. B., Waterman-Storer, C. M., Valdivielso, J. M. and del Pozo, M. A. (2007). Caveolin-1 regulates cell polarization and directional migration through Src kinase and Rho GTPases. *J. Cell Biol.* **177**, 683-694.

Grigoriev, I., Splinter, D., Keijzer, N., Wulf, P. S., Demmers, J., Ohtsuka, T., Modesti, M., Maly, I. V., Grosveld, F., Hoogenraad, C. C. et al. (2007). Rab6 regulates transport and targeting of exocytotic carriers. *Dev. Cell* **13**, 305-314.

Hemler, M. E., Sanchez-Madrid, F., Flotte, T. J., Krensky, A. M., Burakoff, S. J., Bhan, A. K., Springer, T. A. and Strominger, J. L. (1984). Glycoproteins of 210,000 and 130,000 m.w. on activated T cells: cell distribution and antigenic relation to components on resting cells and T cell lines. *J. Immunol.* **132**, 3011-3018.

Hewlett, L. J., Prescott, A. R. and Watts, C. (1994). The coated pit and macropinocytic pathways serve distinct endosome populations. *J. Cell Biol.* **124**, 689-703.

Hida, Y. and Ohtsuka, T. (2010). CAST and ELKS proteins: structural and functional determinants of the presynaptic active zone. *J. Biochem.* **148**, 131-137.

Hotta, A., Kawakatsu, T., Nakatani, T., Sato, T., Matsui, C., Sukezane, T., Akagi, T., Hamaji, T., Grigoriev, I., Akhmanova, A. et al. (2010). Laminin-based cell adhesion anchors microtubule plus ends to the epithelial cell basal cortex through LL5α/beta. *J. Cell Biol.* **189**, 901-917.

Howes, M. T., Kirkham, M., Riches, J., Cortese, K., Walser, P. J., Simpson, F., Hill, M. M., Jones, A., Lundmark, R., Lindsay, M. R. et al. (2010). Clathrin-independent carriers form a high capacity endocytic sorting system at the leading edge of migrating cells. *J. Cell Biol.* **190**, 675-691.

Inoue, E., Deguchi-Tawarada, M., Takao-Rikitsu, E., Inoue, M., Kitajima, I., Ohtsuka, T. and Takai, Y. (2006). ELKS, a protein structurally related to the active zone protein CAST, is involved in Ca2+-dependent exocytosis from PC12 cells. *Genes Cells* **11**, 659-672.

Kishi, M., Kummer, T. T., Eglen, S. J. and Sanes, J. R. (2005). LL5beta: a regulator of postsynaptic differentiation identified in a screen for synaptically enriched transcripts at the neuromuscular junction. *J. Cell Biol.* **169**, 355-366.

Ko, J., Na, M., Kim, S., Lee, J. R. and Kim, E. (2003). Interaction of the ERC family of RIM-binding proteins with the liprin-alpha family of multidomain proteins. *J. Biol. Chem.* **278**, 42377-42385.

Lansbergen, G., Grigoriev, I., Mimori-Kiyosue, Y., Ohtsuka, T., Higa, S., Kitajima, I., Demmers, J., Galjart, N., Houtsmuller, A. B., Grosveld, F. et al. (2006). CLASPs attach microtubule plus ends to the cell cortex through a complex with LL5beta. *Dev. Cell* **11**, 21-32.

Lenter, M., Uhlig, H., Hamann, A., Jenö, P., Imhof, B. and Vestweber, D. (1993). A monoclonal antibody against an activation epitope on mouse integrin chain beta 1 blocks adhesion of lymphocytes to the endothelial integrin alpha 6 beta 1. *Proc. Natl. Acad. Sci. USA* **90**, 9051-9055.

Ludwig, T., Griffiths, G. and Hoflack, B. (1991). Distribution of newly synthesized lysosomal enzymes in the endocytic pathway of normal rat kidney cells. *J. Cell Biol.* **115**, 1561-1572.

Margadant, C., Kreft, M., de Groot, D. J., Norman, J. C. and Sonnenberg, A. (2012). Distinct roles of talin and kindlin in regulating integrin α5β1 function and trafficking. *Curr. Biol.* **22**, 1554-1563.

Monier, S., Jollivet, F., Janoueix-Lerosey, I., Johannes, L. and Goud, B. (2002). Characterization of novel Rab6-interacting proteins involved in endosome-to-TGN transport. *Traffic* **3**, 289-297.

Nakata, T., Kitamura, Y., Shimizu, K., Tanaka, S., Fujimori, M., Yokoyama, S., Ito, K. and Emi, M. (1999). Fusion of a novel gene, ELKS, to RET due to translocation t(10;12)(q11;p13) in a papillary thyroid carcinoma. *Genes Chromosomes Cancer* **25**, 97-103.

Ng, T., Shima, D., Squire, A., Bastiaens, P. I., Gschmeissner, S., Humphries, M. J. and Parker, P. J. (1999). PKCalpha regulates beta1 integrin-dependent cell motility through association and control of integrin traffic. *EMBO J.* **18**, 3909-3923.

Nomura, H., Tadokoro, S. and Hirashima, N. (2011). Liprin-α is involved in exocytosis and cell spreading in mast cells. *Immunol. Lett.* **139**, 110-116.

Paranavitane, V., Coadwell, W. J., Eguinoa, A., Hawkins, P. T. and Stephens, L. (2003). LL5β is a phosphatidylinositol (3,4,5)-trisphosphate sensor that can bind the cytoskeletal adaptor, gamma-filamin. *J. Biol. Chem.* **278**, 1328-1335.

Paranavitane, V., Stephens, L. R. and Hawkins, P. T. (2007). Structural determinants of LL5beta subcellular localisation and association with filamin C. *Cell. Signal.* **19**, 817-824.

Pellinen, T., Tuomi, S., Arjonen, A., Wolf, M., Edgren, H., Meyer, H., Grosse, R., Kitzing, T., Rantala, J. K., Kallioniemi, O. et al. (2008). Integrin trafficking regulated by Rab21 is necessary for cytokinesis. *Dev. Cell* **15**, 371-385.

Rezaul, K., Thumar, J. K., Lundgren, D. H., Eng, J. K., Claffey, K. P., Wilson, L. and Han, D. K. (2010). Differential protein expression profiles in estrogen receptor-positive and -negative breast cancer tissues using label-free quantitative proteomics. *Genes Cancer* **1**, 251-271.

Roberts, M., Barry, S., Woods, A., van der Sluijs, P. and Norman, J. (2001). PDGF-regulated rab4-dependent recycling of alphavbeta3 integrin from early endosomes is necessary for cell adhesion and spreading. *Curr. Biol.* **11**, 1392-1402.

Sahai, E. (2007). Illuminating the metastatic process. *Nat. Rev. Cancer* **7**, 737-749.

Shi, F. and Sottile, J. (2008). Caveolin-1-dependent beta1 integrin endocytosis is a critical regulator of fibronectin turnover. *J. Cell Sci.* **121**, 2360-2371.

Stryker, E. and Johnson, K. G. (2007). LAR, liprin alpha and the regulation of active zone morphogenesis. *J. Cell Sci.* **120**, 3723-3728.

Südhof, T. C. (2012). The presynaptic active zone. *Neuron* **75**, 11-25.

Takabayashi, T., Xie, M. J., Takeuchi, S., Kawasaki, M., Yagi, H., Okamoto, M., Tariqur, R. M., Malik, F., Kuroda, K., Kubota, C. et al. (2010). LL5β directs the translocation of filamin A and SHIP2 to sites of phosphatidylinositol 3,4,5-triphosphate (PtdIns(3,4,5)P3) accumulation, and PtdIns(3,4,5)P3 localization is mutually modified by co-recruited SHIP2. *J. Biol. Chem.* **285**, 16155-16165.

Tomaselli, K. J., Damsky, C. H. and Reichardt, L. F. (1988). Purification and characterization of mammalian integrins expressed by a rat neuronal cell line (PC12): evidence that they function as alpha/beta heterodimeric receptors for laminin and type IV collagen. *J. Cell Biol.* **107**, 1241-1252.

Totaro, A., Paris, S., Asperti, C. and de Curtis, I. (2007). Identification of an intramolecular interaction important for the regulation of GIT1 functions. *Mol. Biol. Cell* **18**, 5124-5138.

Valdembri, D. and Serini, G. (2012). Regulation of adhesion site dynamics by integrin traffic. *Curr. Opin. Cell Biol.* **24**, 582-591.

Valdembri, D., Caswell, P. T., Anderson, K. I., Schwarz, J. P., König, I., Astanina, E., Caccavari, F., Norman, J. C., Humphries, M. J., Bussolino, F. et al. (2009). Neuropilin-1/GIPC1 signaling regulates alpha5beta1 integrin traffic and function in endothelial cells. *PLoS Biol.* **7**, e25.

van der Vaart, B., van Riel, W. E., Doodhi, H., Kevenaar, J. T., Katrukha, E. A., Gumy, L., Bouchet, B. P., Grigoriev, I., Spangler, S. A., Yu, K. L. et al. (2013). CFEOM1-associated kinesin KIF21A is a cortical microtubule growth inhibitor. *Dev. Cell* **27**, 145-160.

Vicente-Manzanares, M., Choi, C. K. and Horwitz, A. R. (2009). Integrins in cell migration – the actin connection. *J. Cell Sci.* **122**, 199-206.

Wang, Y., Liu, X., Biederer, T. and Südhof, T. C. (2002). A family of RIM-binding proteins regulated by alternative splicing: Implications for the genesis of synaptic active zones. *Proc. Natl. Acad. Sci. USA* **99**, 14464-14469.